Supplementary File –Water as Additive Directing Lithium Electrodeposition

Mark Aarts, Sai Gourang Patnaik, Toon Van Roy, Stefanie Sergeant, Maarten Debucquoy, Philippe M. Vereecken

SI-1 Methods

Equipment

Electrochemical experiments were conducted in an Argon-filled glovebox (MBraun), using an Autolab potentiostat (PGSTAT30) for experiments on stationary electrodes and a Biologic bipotentiostat (VSP-300) for the RRDE experiments. The homemade electrochemical cells consist of Teflon and include 2 compartments for the reference and counter electrode, respectively, connected by a Luggin capillary. The electrochemical cell was clamped on top of the working electrode and sealed with an O-ring (Kalrez, compound 6375, DuPont). The cells were cleaned using acid piranha (1:3 hydrogen peroxide, 30%, KMG chemicals : Sulfuric acid, 96%, CMC materials) every time a different electrolyte was used, and regularly when using the same electrolyte. Electrolytes were prepared and stored in glassware with a Teflon-coated stirring magnet, all of which were cleaned with acid piranha and brought into the glovebox after vacuum drying at 100° C for several hours before first use.

For the RRDE experiments an MSR rotator was used with an E6R1 ChangeDisk electrode (Cu disk, Pt ring, Pine Research). The electrode was rotated at 100 rpm. A glass beaker was used for the RRDE experiments, which was cleaned with acid piranha before every experiment and brought into the glovebox after vacuum drying in the antechamber (no heating). After every experiment the RRDE was polished on a rotating table with a polishing cloth and sequentially using a 3 µm, 1 µm, and 0.25 µm diamond suspension (Dia-complete poly, QATM).

SEM images were made using a NOVA200 near the center of the sample, after cleaving samples in half.

Electrochemical experiments

Sputter-coated copper on silicon wafers was used as a working electrode (150 nm copper on top of a 10 nm titanium adhesion layer on boron doped silicon, ρ = 1-30 Ωm, Si-Mat). Samples were prepared by cleaving the wafer and cleaned with isopropanol. Samples were contacted from the top by folding aluminium foil around the edges, outside the region of the O-ring, which were then placed on a conducting base for contacting the potentiostat. Metallic lithium ribbon was used as counter-, and reference electrodes (99.9%, Sigma-Aldrich), which was scraped clean using a toothbrush before use.

Lithium bis(trifluoromethanesulfonyl)imide (LiTFSI, 99.9% under Argon, Solvionic) and $LiClO_4$ (99.99%, battery grade, dry, Sigma-Aldrich) were used as electrolytes in tetraethylene glycol dimethyl ether (4G, 99%, Sigma-Aldrich), which was dried over 4 Å molecular sieves before use (Thermo Scientific). This solvent is mainly selected for its high boiling point and the electrochemical stability of ether solvents[1].The water additive was produced at high purity (18.2 MΩ·cm), but stored in a buffertank without a nitrogen

blanket. Prior to all ex-situ imaging (SEM, photos, AFM) samples were rinsed with propylene carbonate (99.7% anhydrous, Sigma-Aldrich) and dried in vacuum.

Atomic Force Microscopy

The AFM topography images were obtained using a Bruker Dimension Icon operating in Pulsed Force mode. The AFM tool is located in a N_2/Ar filled glovebox to prevent changes to the sample's surface as result of ambient exposure. All samples were transferred to the AFM glovebox in an airtight sealed container. A HQ-NSC19/AlBs probe with a tip radius of 8 nm and a spring constant of 0.5 N/m was used for the measurements. A low spring constant cantilever is preferred to minimize hard tip-sample interactions to avoid changes to the sample's surface. When Li was present on the sample's surface, a metal coated tip (PPP-EFM) with a tip radius of 25 nm and a spring constant of 2.8 N/m was used instead due to the reactivity of Li with Si and SiN.

SI-2 Growth characteristics for lithium deposited from LiTFSI and $LiClO_4$ salts at varying experimental conditions.

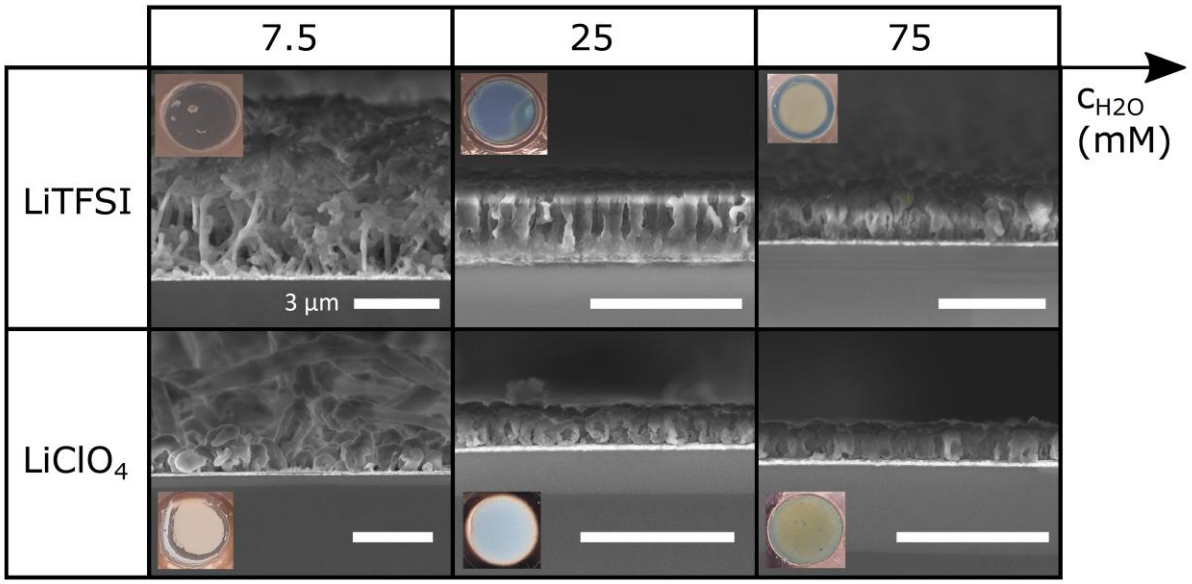

Figure S1: Cross-sectional SEM images for the samples shown in Figure 1 in the main text, after plating -0.74 C/cm^2 at -1 mA/cm^2 using 1 M LiTFSI or 1 M $LiClO_4$ + *x* mM H_2O (4G). All scale bars are 3 µm. Insets shows digital photos of the samples.

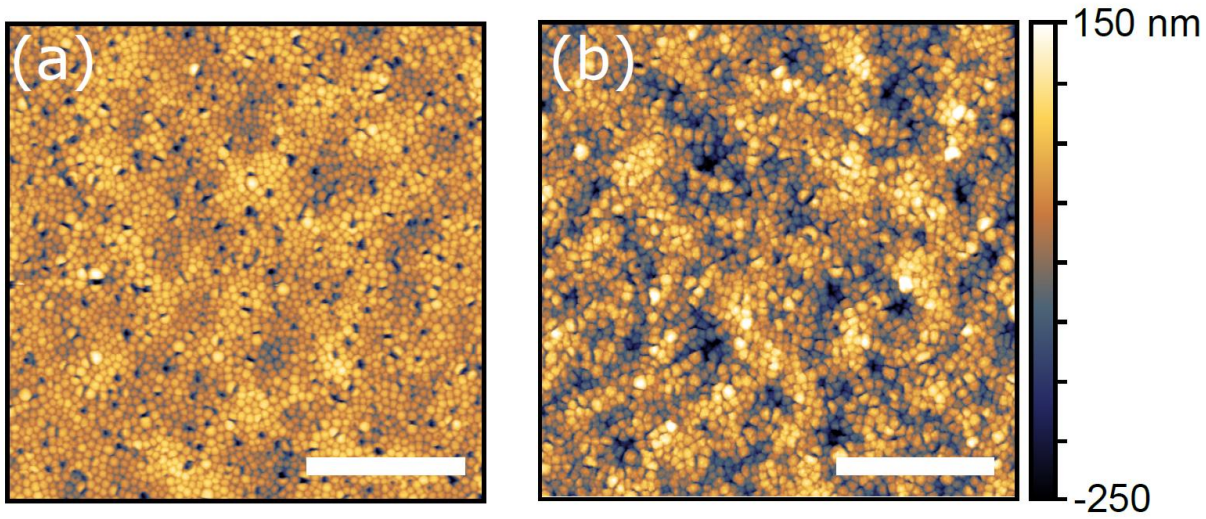

Figure S2: *ex-situ* AFM images in a glovebox environment of 1 µm lithium deposited from (a) 1 M LiTFSI + 25 mM H_2O (4G). RMS roughness is 46 nm. (b) 1 M $LiClO_4$ + 25 mM H_2O (4G). RMS roughness is 65 nm. Scale bars are 5 µm. It is worth mentioning that some columns appear open/hollow in the AFM images, as well as in the SEM images in Figures S1 and Figure 1 in the main text. Analogous to our conclusions, similar morphologies have been attributed to hydrogen evolution during electrodeposition[2,3].

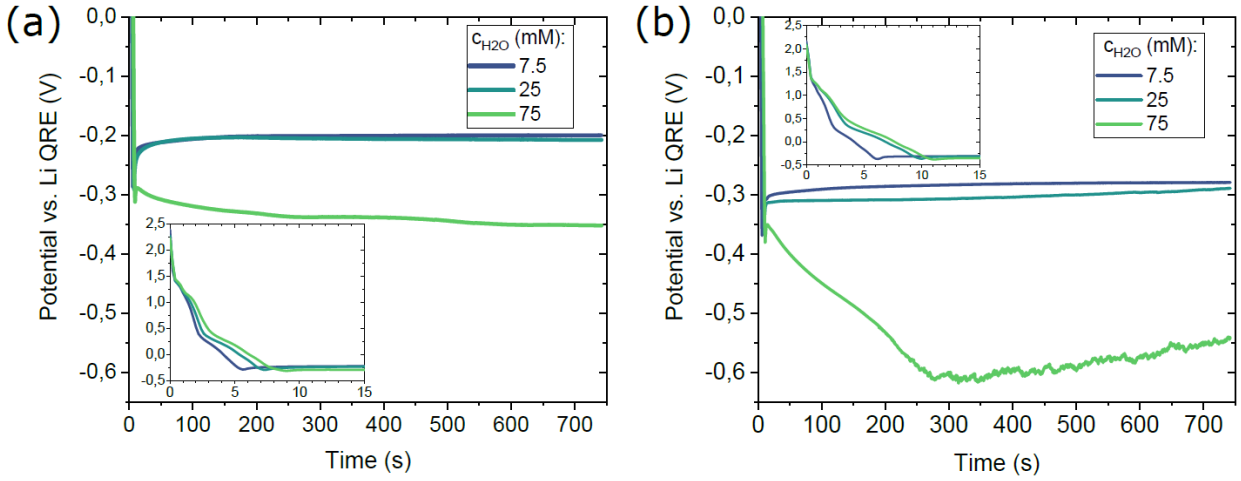

Figure S3: V-t traces for the samples shown in Figure 1 in the main text for (a) 1 M LiTFSI + *x* mM H_2O, and (b) 1 M LiClO4 + *x* mM H_2O. The insets show the first 15 seconds of the trace (nucleation), the y-axis runs from -0.5 to 2.5 V.

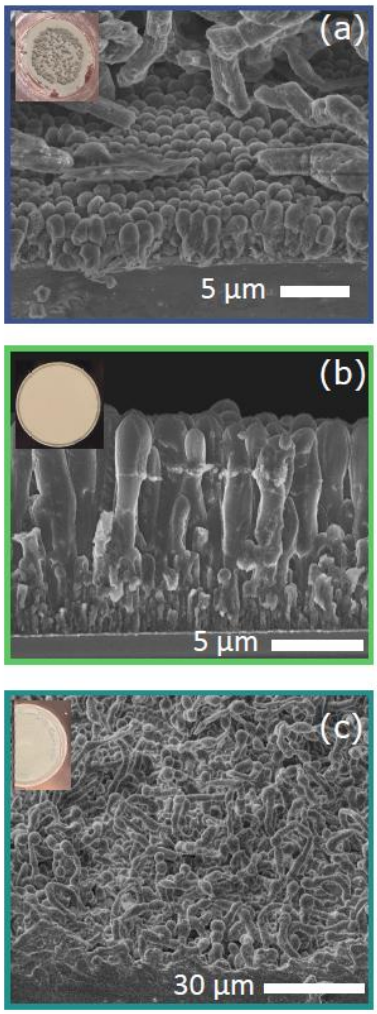

Figure S4: Illustration of columnar morphologies obtained when scaling the additive concentration with the plating current density. (a) 7.5 mM H_2O at -0.3 mA/cm^2 (45° sample tilt). (b) 75 mM H_2O at -3 mA/cm^2 (90° sample tilt). (c) 25 mM H_2O at -3 mA/cm^2 (45° sample tilt). Columns are observed for the first 2 conditions. It is worth pointing out that in both these cases the column diameter is much larger than for the conditions used in Figure 2 in the main text, such that the samples did not display any bright colors. A poorly directed mossy growth is again obtained in the last image, when increasing the current density to -3 mA/cm^2 in the electrolyte with 25 mM H_2O.

SI-3. Cyclic voltammetry and linear sweep voltammetry at various water concentrations.

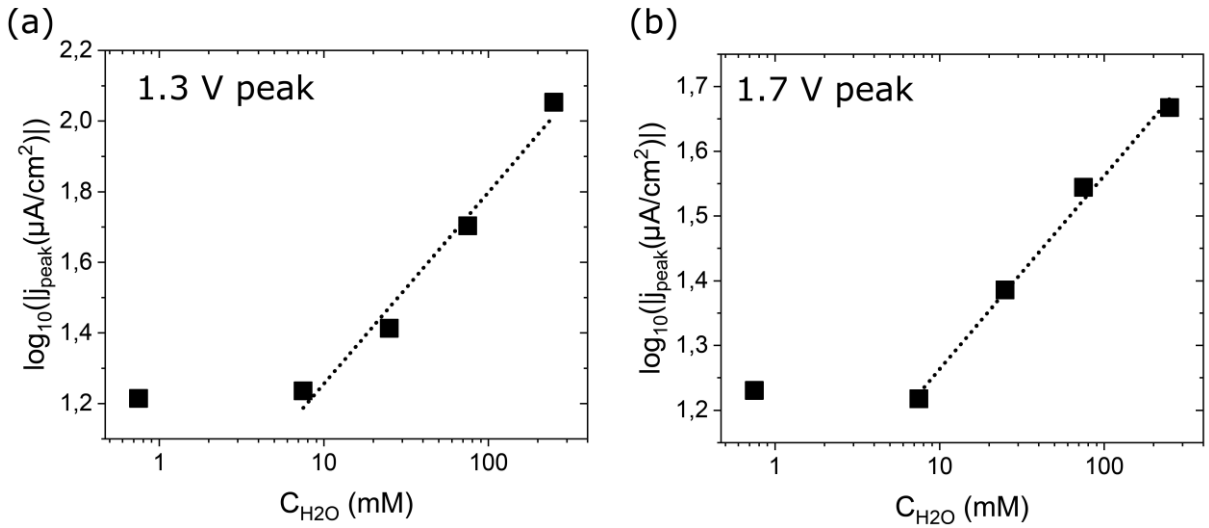

Figure S5: Evolution of the peak current density for the H_2O-dependent peaks in the Linear Sweep Voltammogram in Figure 3(a) in the main text as a function of H_2O concentration (logarithmic axes). (a) ~1.3 V peak (b) ~1.7 V peak. We estimate the reaction order from the slope of the peak current densities for $C_{H2O} \geq 7.5$ mM (linear fit on the log-log scale indicated by the dashed line) to be ~0.54 and ~0.30 for the 1.3 V and the 1.7 V peak, respectively. This reaction order for the 1.3 V peak is the same as the one obtained recently by Martins *et al.*[4]. We attribute the deviation from the linear relation at 0.75 mM to limitations of our drying procedure.

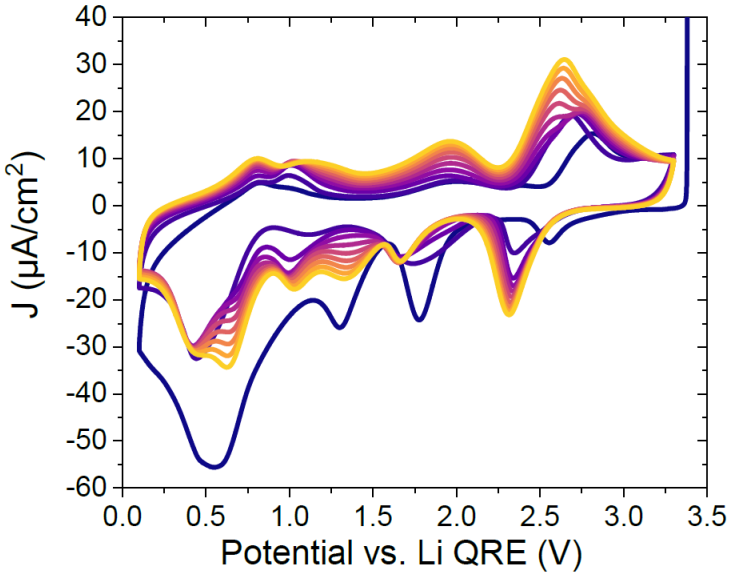

Figure S6: Cyclic voltammogram (10 cycles, from purple to orange) with 25 mM H_2O at 5 mV/s. The behavior of the peaks at ~1.3 V and ~1.7 V as a function of added water in the first cycle is consistent with the results of Aurbach *et al.*[5] upon the addition of water, where it should be noted that the peak around ~1.7 V was also affected by the presence of oxygen in that work (see methods). Strikingly, we observe that the peak at ~1.3 V is passivated in the second cycle, as in reference[5], but reappears and splits in subsequent cycles.

SI-4. Ex-situ AFM images and statistics after potential-hold formation experiments.

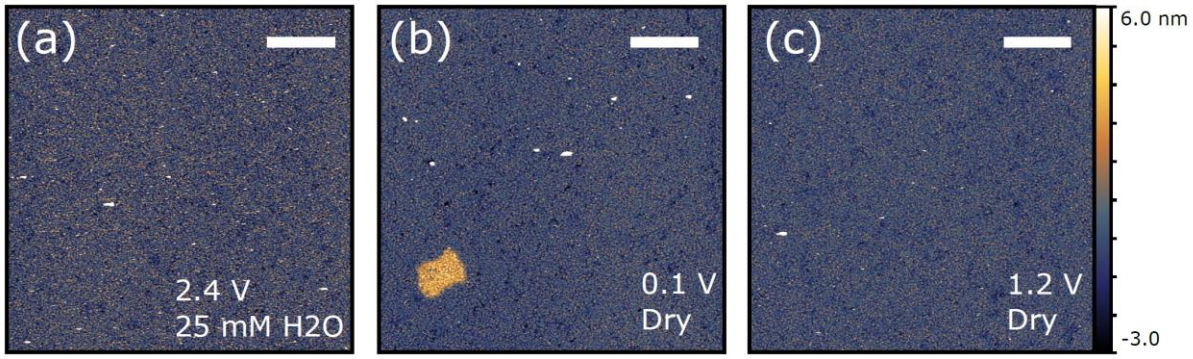

Figure S7: Complementary ex-situ AFM images to Figure 3b in the main text, where the sample is kept at a specific potential in 1 M LiTFSI + *x* mM H_2O until the charge setpoint of -10 mC/cm^2 is reached. (a) Sample kept at 2.4 V with 25 mM H_2O. (b) Sample kept at 0.1 V in the dried electrolyte. (c) Sample kept at 1.2 V in the dried electrolyte. Little to no features are observed on these sample, where the patch at 0.1 V was the only one seen at these conditions (see Table S1). The scale bars are 2 µm.

Table S1 Patch density obtained from AFM: Density of patches as the one shown in Figure S7 and Figure 3b in the main text.

c_{H2O} / V_{hold}	Amount of patches	Area scanned (µm^2)	Density (patches/ µm^2)
25 mM / 2.4 V	0	325	0
25 mM / 1.7 V	0	325	0
25 mM / 1.2 V	15	325	46.1e-3
Dry / 1.2 V	0	300	0
25 mM / 0.1 V	4	625	6.4e-3
Dry / 0.1 V	1	400	2.5e-3

Table S2. Potential-hold time: Time to reach -10 mC/cm^2 in potential-hold formation for samples used in Figure 3b in the main text and Figure S7. Slashes indicate different samples.

c_{H2O} / V_{hold}	Time to reach -10 mC/cm^2
25 mM / 2.4 V	1071 s / 9778 s
25 mM / 1.7 V	5841 s / 269 s / 827 s
Dry / 1.2 V	358 s
25 mM / 1.2 V	566 s / 647 s
Dry / 0.1 V	62 s
25 mM / 0.1 V	66 s / 55 s / 26 s

SI-5. Deposition from dry electrolyte after potentiostatic formation with 25 mM H_2O.

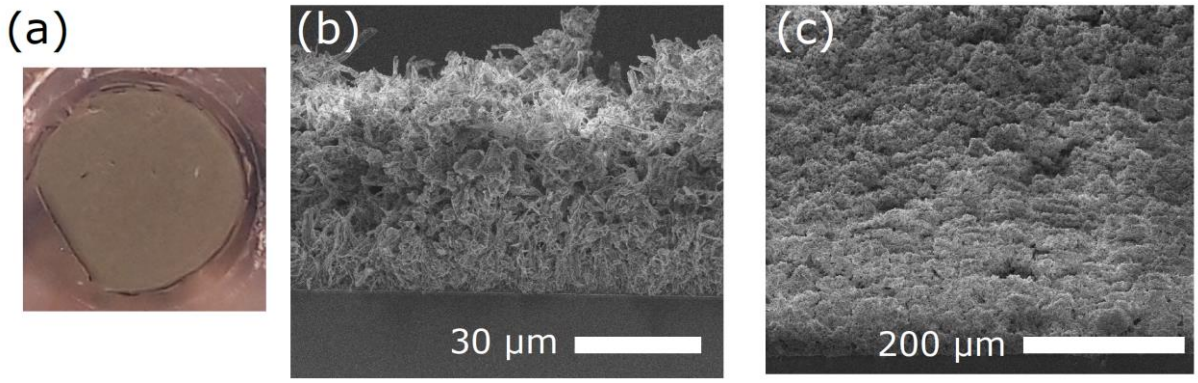

Figure S8: Sample after galvanostatic electroplating of -7.4 C/cm^2 in dry 1 M LiTFSI (4G), after formation at 0 V until a total charge of -21 mC/cm^2, ~3x the amount of charge after the galvanostatic formation until 0 V as shown in Figure 4b in the main text. (a) Digital photo of the sample after plating. (b) Cross-sectional SEM. (c) SEM, 45° sample tilt. The appearance of the sample is very similar to the one obtained with galvanostatic cycling until 0 V. Clearly no columnar growth is observed.

SI-6. Additional RRDE data.

Figure S9: Digital photo of the RRDE after electroplating at 100 rpm in the dried electrolyte. In this case the procedure consisted of 3 steps; i) Cyclic voltammetry between 3.0 V and 0.1 V for 3 cycles (5 mV/s). ii) Galvanostatic plating at j_{disk} = -1 mA/cm^2 for 742 s. iii) Relaxation at j_{disk} = 0 mA/cm^2.

Contrastingly to the stationary electrode (Figure 4a in the main text) a greyish/black deposit is observed on the copper disk electrode, similar to the deposition in Figure 1 in the main text at low added H_2O concentrations. We attribute this to the rotation driving additional H_2O towards the interface during deposition. Effectively, this implies that we cannot get rid of all the water under rotation. Additionally, the experiment could be affected by water impurities introduced by the glass beaker used for the RRDE experiments, which was dried in the glovebox antechamber without heating when bringing it inside. The dark appearance of the platinum ring is an artifact due to the reflection at this angle.

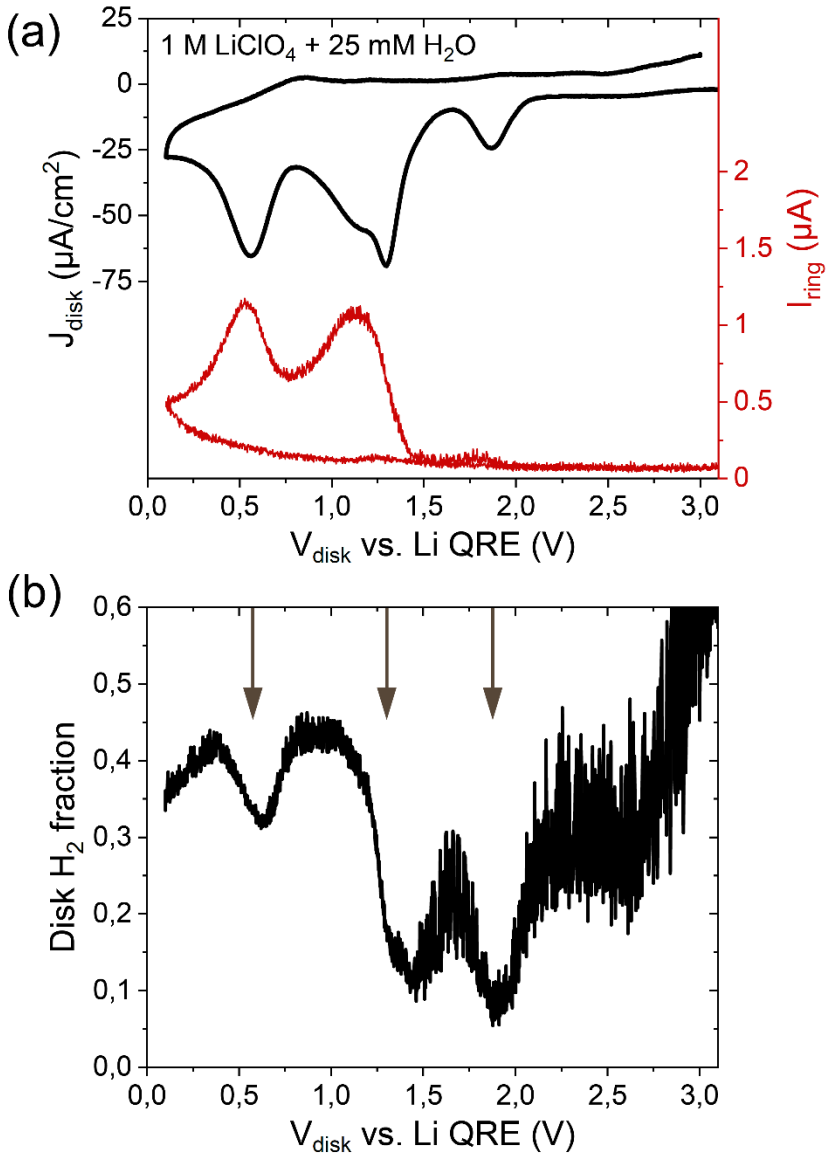

Figure S10: (a) First cycle of a cyclic voltammogram in 1 M $LiClO_4$ + 25 mM H_2O (4G) using the Cu disk and Pt ring RRDE, scanned from OCP to 0.1 V at 5 mV/s. The ring is kept at 3.5 V. Disk current density is shown in black (top, left axis), and ring current in red (bottom, right axis) (b) Fraction of generated hydrogen on the disk calculated as $\left|\frac{I_{ring}}{I_{disk}*0.256}\right|$, using the electrode efficiency of 25.6%. Arrows indicate the peaks in the disk current from image (a). The behavior of the $LiClO_4$ electrolyte is qualitatively the same as for the LiTFSI electrolyte shown in Figure 6 in the main text.

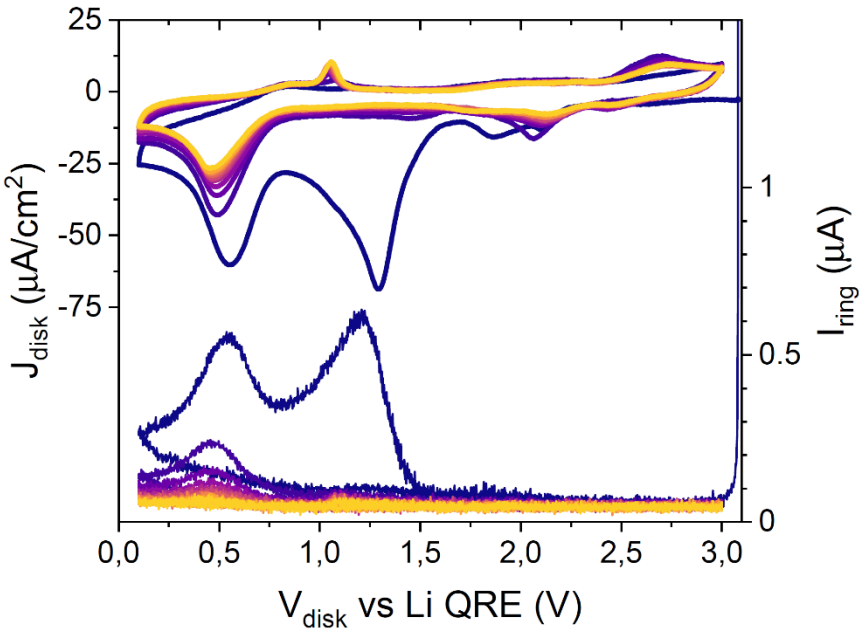

Figure S11: Cyclic voltammetry for 10 cycles (purple to orange) between 3.0 V and 0.1 V at 5 mV/s for the RRDE rotated at 100 rpm in 1 M LiTFSI + 25 mM H_2O (4G) showing disk current density (top, left axis) and ring current (bottom, right axis). The ring was kept at 3.5 V during the experiment. All ring currents rapidly passivate after the first cycle. Furthermore, splitting and shifting of the peaks on the disk as observed on the stationary electrode (Figure S6) is not seen on the RRDE. Here, almost all disk current disappears after multiple cycles, except for the peak at 0.5 V.

SI-7. Table of free energies and potential reactions.

Table S3. Table of free energies

Compound	Gibbs Free Energy (kJ/mol)
H_2	0
H_2O (l)	-237.14
HF(g)	-277.3
Li^+ (aq)	-293.3
LiF	-587.7
LiH	-68.45
Li_2O	-561.2
LiOH	-439
OH^-(aq)	-157.28

The following potential reactions are considered (reactions mentioned in main text in boldface). Estimations for standard potentials vs. Li^+/Li are calculated with the values from Table S3 obtained from Lange's handbook of chemistry[6], using $U_0 = 3.04 + \Delta G * 10^3/(-n * F)$ with *n* the amount of electrons in the reaction, and *F* the Faraday constant. Note that the values in Table S3 may differ from the actual values in the employed electrolyte system, due to e.g. the different solvent. Similarly, the applied potentials can shift depending on the electrolyte system due to the use of a Lithium QRE[7].

$\boldsymbol{2HF + 2Li^+ + 2e^- \rightarrow 2LiF + H_2}$	**U_0 = 3.22 V**	**vs. Li^+/Li**	**(1)**
$2H_2O + 2e^- \rightarrow 2\,OH^- + H_2$	U_0 = 2.21 V		(2)
$\boldsymbol{2H_2O + 2Li^+ + 2e^- \rightarrow 2LiOH + H_2}$	**U_0 = 2.09 V**		**(3)**
$\boldsymbol{H_2O + 2Li^+ + 2e^- \rightarrow Li_2O + H_2}$	**U_0 = 1.68 V**		**(4)**
$H_2O + 2Li^+ + 2e^- \rightarrow LiOH + LiH$	U_0 = 1.40 V		(5)
$\boldsymbol{2LiOH + 2Li^+ + 2e^- \rightarrow 2Li_2O + H_2}$	**U_0 = 1.27 V**		**(6)**
$H_2O + 4Li^+ + 2e^- \rightarrow Li_2O + LiH$	U_0 = 1.19 V		(7)
$2Li^+ + H_2 + 2e^- \rightarrow 2LiH$	U_0 = 0.71 V		(8)

SI-8. Column stripping behavior.

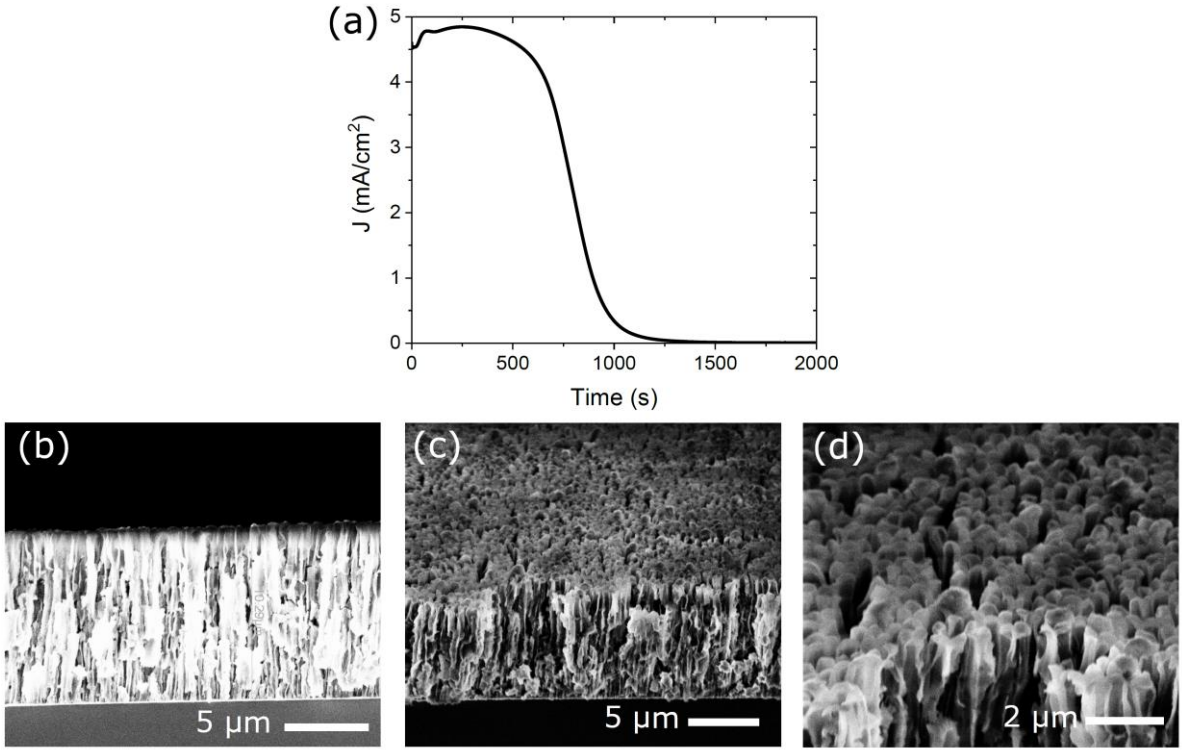

Figure S12: (a) Current density-time trace when applying 1 V immediately after galvanostatic electrodeposition of -7.42 C/cm^2 (10 µm) of lithium at -1 mA/cm^2 using a 1 M LiTFSI + 25 mM H_2O electrolyte. The current density is ~4.5 mA/cm^2 before rapidly decreasing after ~10 min. The total extracted charge is ~3.8 C/cm^2 (~50% of the deposited charge). (b-d) SEM images of the cleaved sample following the stripping, at (b) 90° and (c-d) 45° sample tilt. The columnar structure is retained, and the thickness of the layer is still determined to be ~10 µm. Imaging showed very noticeable charging in this case. We cannot determine from these images whether this is due to all the remaining material being non-conducting, or whether parts of the column get electrically disconnected from the substrate during stripping.

References

1. Park, M. S. *et al.* A highly reversible lithium metal anode. *Sci. Rep.* **4**, 1–8 (2014).

2. Fan, Y. W. & Wang, R. Z. Submicrometer-Sized Vaterite Tubes Formed Through Nanobubble-Templated Crystal Growth. *Adv. Mater.* **17**, 2384–2388 (2005).

3. Saadat, S. *et al.* Template free electrochemical deposition of ZnSb nanotubes for Li ion battery anodes. *Chem. Commun.* **47**, 9849 (2011).

4. Martins, M. *et al.* Role of Catalytic Conversions of Ethylene Carbonate, Water, and HF in Forming the Solid-Electrolyte Interphase of Li-Ion Batteries. *ACS Catal.* **13**, 9289–9301 (2023).

5. Aurbach, D., Daroux, M., Faguy, P. & Yeager, E. The electrochemistry of noble metal electrodes in aprotic organic solvents containing lithium salts. *J. Electroanal. Chem. Interfacial Electrochem.* **297**, 225–244 (1991).

6. *Lange's Handbook of Chemistry*, McGraw-Hill: 2005, 16th edition

7. Ko, S. *et al.* Electrode potential influences the reversibility of lithium-metal anodes. *Nat. Energy* **7**, 1217–1224 (2022).